RSC Advances

ROYAL SOCIETY OF CHEMISTRY

www.rsc.org/advances

Journal Name

RSCPublishing

COMMUNICATION

Amorphous titanate-crosslinking N-rich carbon hybrid with 3D channels for fast lithium storage

Cite this: DOI: 10.1039/x0xx00000x

Jiehua Liu,[a]* Jiaqi Xu,[a] Kuan Zhou,[a] Lei Wang [b] and Xiangfeng Wei [ac]

Received 00th January 2012,
Accepted 00th January 2012

DOI: 10.1039/x0xx00000x

www.rsc.org/

Carbon-based anodes are considered as the preferred choice owing to their unique properties, but they are limited by high-rate performance and capacities. To overcome the volume swell of layered materials like graphite, a novel amorphous titanate-crosslinking N-rich carbon hybrid is successfully prepared by a facile one-pot method for the first time. Due to stable 3D framework with good distribution of nitrogen and titanium, the obtained hybrid demonstrates a high reversible capacity of 523.3 mA h g^{-1} at high rate of 2 A g^{-1}, much higher than theoretical value (372 mA h g^{-1}) of layered graphite. This hybrid anode also exhibits superior high-rate capability and cycling performance, possibly serving as a novel sustainable material for lithium-ion batteries and supercapacitors.

Introduction

Carbon-based anode is considered as the preferred choice for next-generation lithium-ion batteries (LIBs) because of its structural, thermal and electronic properties.[1-3] Compare to the rapid development of cathodes, the high-performance anode materials are still urgently needed.[4-6] Lithium-storage performance of anode is one of the most important factors contributing to higher energy density, power density and shortened charging time. To meet the market requirements, lithium capacity, rate performance and cost are three major considerations in the context of advanced LIB with carbon-based anode materials. For example, carbon nanotubes with 1D structure are limited in widely application due to high cost and small scale production.[7, 8] Graphite as one of important carbon materials with 2D channel has been widely employed in commercial LIBs due to its high theoretical capacity of 372 mA h g^{-1}, but it often exhibits poor cycling performance and low capacity at high rates because of the structural swell limitation.[9, 10]

Nitrogen-rich 1D or 2D carbon materials also exhibit improved capacities for lithium storage, but the high costs of these hybrids using carbon-based materials and the complex process restrict their extensive applications.[11, 12] Titanium based anode materials exhibit stable structure contributing excellent performance for fast lithium storage, such as sandwich-like titanate nanosheets [13, 14] and lithium titanate [15, 16]. However, their relatively-low capacities and anode potential make them less competitive in LIBs. To overcome the shortcomings, titanate/carbon composites were fabricated with improving performances with a synergistic effect.[17, 18] However, most of titanates employed in the composites are crystal structures, which still limited the whole capacities of composites. Amorphous composite might have unexpected results for lithium storage, but few results, if have, had appeared about amorphous titanate-carbon hybrid in the literature. We have a great interest in creating new ways to fabricate new structures.

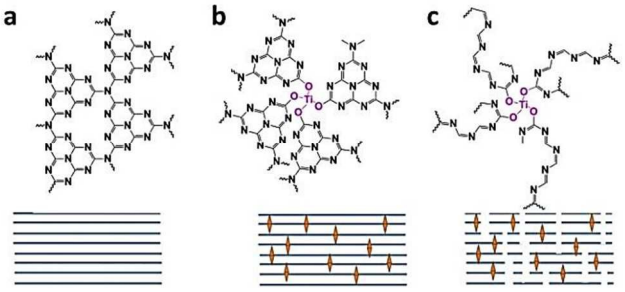

Scheme 1. a) g-C_3N_4 with 2D channels; b) Titanate crosslinking g-C_3N_4 hybrid with 2D channels; c) N-rich carbon/ titanate hybrid with 3D channels.

We noticed that graphitic C_3N_4 (g-C_3N_4) not only has a similar two dimensional nano-architecture with graphite (Scheme 1a), but also exhibits distinctive semiconductor properties.[19-24] However, g-C_3N_4 is often overlooked in the field of energy storage due to its low capacity of lithium storage. The synthesis process of g-C_3N_4 is easier and gentler than that of graphite. Also, substrates (e.g. melamine, urea) with amino groups provide huge potential for developing functional carbon-based materials. To overcome the volume swell of layered materials, crosslinking agents may be employed to improve their stability performance as shown in Scheme 1b. After *in situ* carbonization, the 3D channels will be formed *in situ* (Scheme 1c). The obtained titanate-crosslinking N-rich carbon hybrid (TNCH) with 3D channels may be an alternative host for lithium storage. In this work, the possibility of higher lithium storage capacity was explored by *in situ* one-pot method of fabrication. According to this process, the amorphous material, consisting of carbon, nitrogen and titanate, offers 3D channels for fast Li^+ intercalation. The amorphous hybrid exhibits higher capacities and better rate performance than individual graphite or titanate, and are particularly applicable to fast lithium storage.

Results and discussion

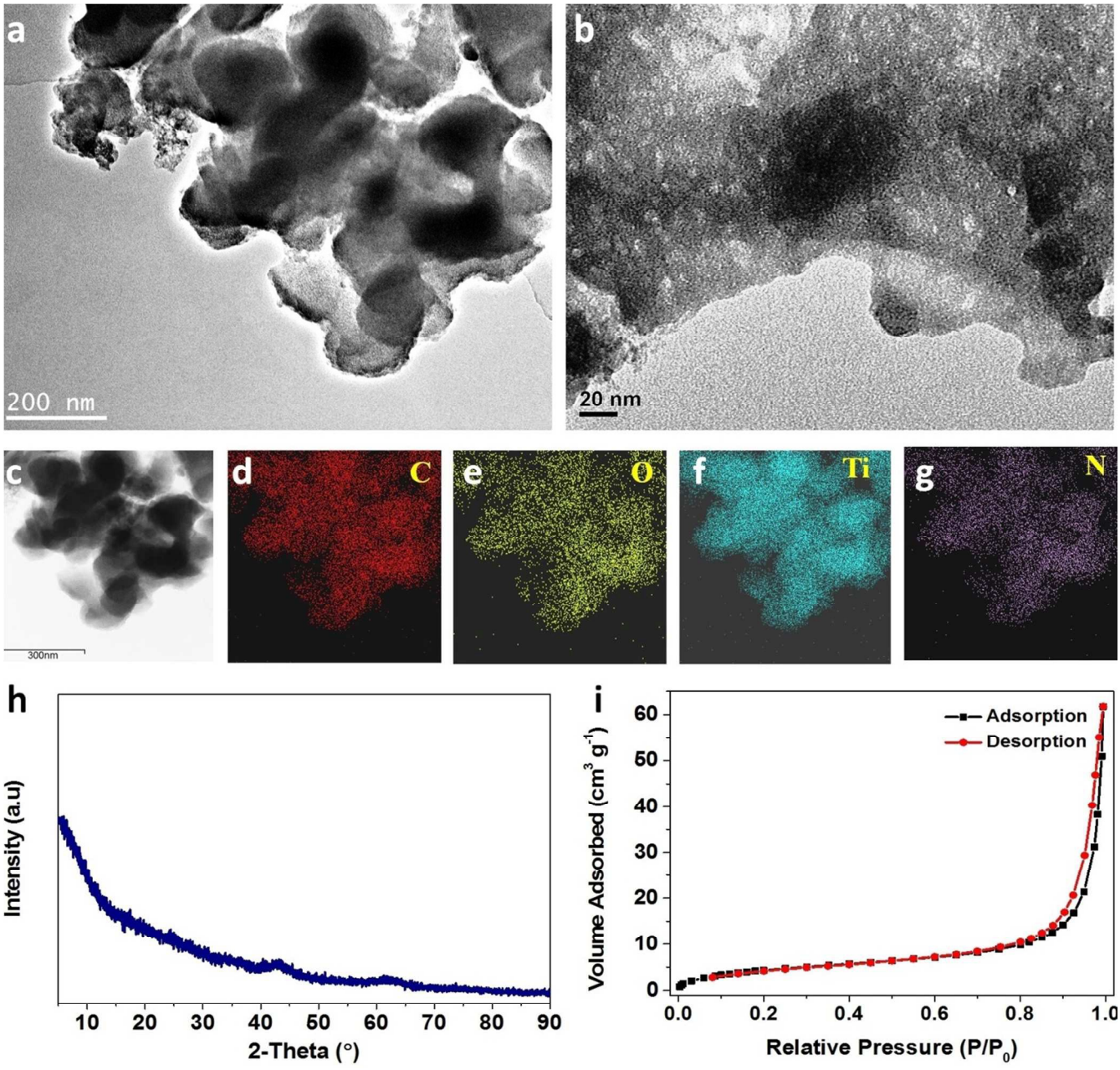

Fig. 1. a and b. TEM images; c−g. STEM image, C, O, Ti, N mappings respectively; h. XRD pattern and i. N_2 adsorption-desorption isotherms of TNCH.

Journal Name

RSCPublishing

COMMUNICATION

Fig. 1a and 1b shows TEM images of the TNCH. Fig. 1a shows an irregular morphology of grains. Fig. 1b provides a direct evidence of proposed 3D structure, which clearly show nanoporous 3D channels. Fig. S1 is HRTEM and Fast Fourier Transform images of the enlarged outer surface in Fig 1a, which are a typical amorphous structure with disordered atomic structure. To further confirm the formation of 3D channels, Fig. S2 shows TEM images of intermediates which were annealed at 500 ºC for 2 hours (Fig. S2a) and 650 ºC for 1 hour (Fig. S2b). There are obvious 3D channels obtained at 650 ºC rather than 500 ºC. STEM image (Fig. 1c) and the corresponding elemental mappings (Fig.1d-g) of C, O, Ti and N revealed that C, O, Ti and N were evenly distributed in the TNCH grains. In Fig.1h, no strong characteristic peak of TNCH was detected in the XRD pattern, which reveals amorphous features and excludes the existence of crystalline TiO_2, graphite and g-C_3N_4 (Fig. S3)[25], which support our proposal in Scheme 1c. A little amount cubic titanium oxide (JCPDS card No: 89-3660) or titanium nitride (JCPDS card No: 87-0627) may be obtained in the reducing atmospheres which were produced by decomposition of C_3N_4. As shown in Fig. 1i, the BET specific surface area of TNCH is 16.8 m^2 g^{-1} and the total pore volume of 0.096 cm^3 g^{-1} has concluded using adsorption data.

Fig. S4 shows Fourier-transform infrared (FT-IR) spectra of g-C_3N_4 and TNCHs, which exhibit the existence of polymeric N-heterocycles. The overall spectra features of g-C_3N_4 obtained at 650 without Ti crosslinking agent are similar to those of the reported g-C_3N_4.[26, 27] The absorption bands centered at 1574 and 1637 cm^{-1} are attributed to C=N stretching, while the multiple bands between 1200 and 1500 cm^{-1} to aromatic C-N stretching. A broad band at 2900−3400 cm^{-1} belong to the stretching modes of $-NH_2$ or =NH groups in agreement with the results from XPS analysis. In particular, all above characteristic absorption peaks in g-C_3N_4 nearly disappear in the spectrum of TNCHs, indicating that g-C_3N_4 structure was destroyed with the catalysis of titanate.

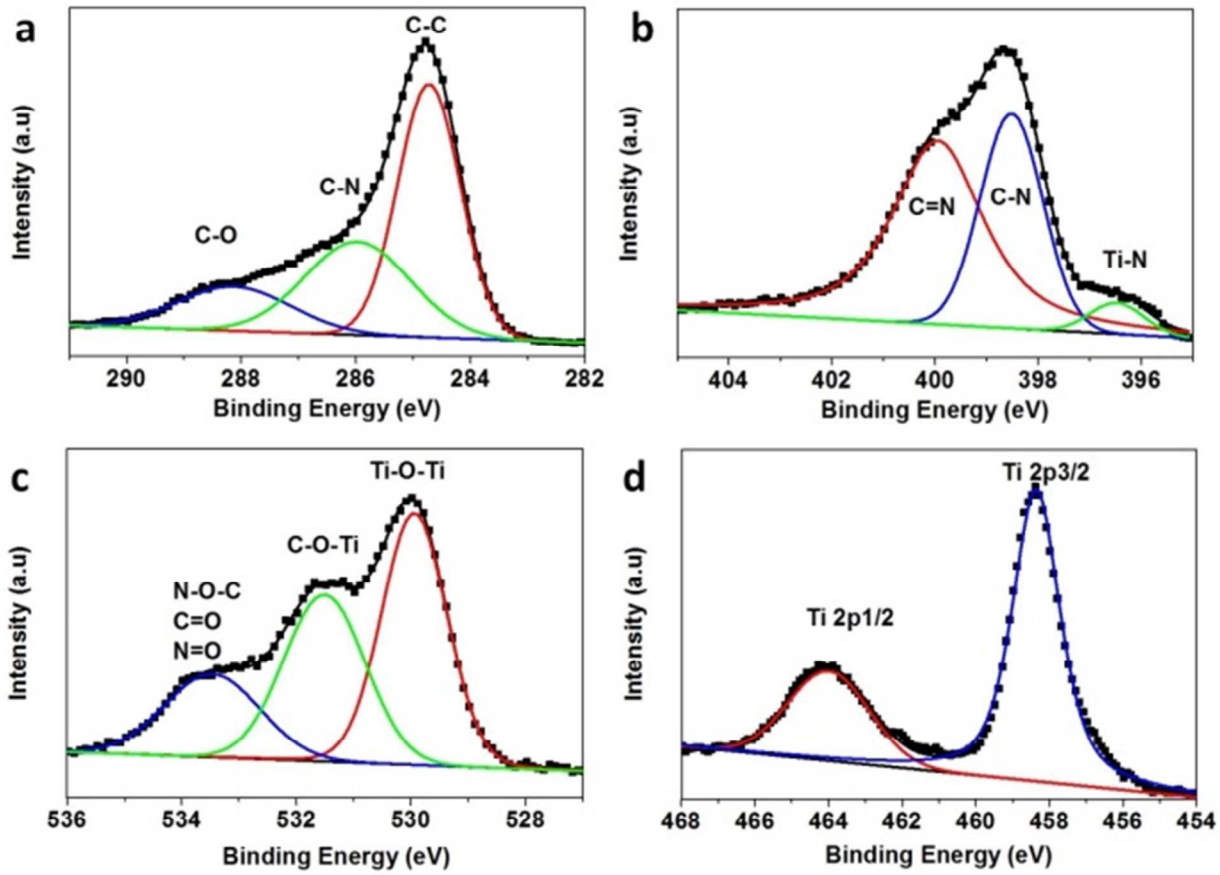

Fig. 2. High resolution XPS spectra a) C1s, b) N1s, c) O1s and d) Ti2p of TNCH.

Journal Name RSCPublishing

COMMUNICATION

XPS measurements were employed to define the chemical environment of the elements based on their binding energy and determined the main components of TNCH. Full XPS spectrum detected the signals for C1s, N1s, O1s and Ti2p in the near surface range of TNCH (Fig. S5). The atomic percentage of C, N, O and Ti are 56.67%, 14.79%, 21.73% and 6.83% respectively. It is worth noting that the ratio of O and Ti in the sample is 3.18 : 1, much higher than the ratio in TiO_2. The possibility is that the melamine reacted with titanic acid to form a new and stable Ti–O–C bond by deamination. The results further prove the role of titanate is the crosslinking agent.

High-resolution XPS spectra were provided in Fig. 2. C1s XPS spectrum indicates the asymmetrical peak, and its deconvolution core level spectrum at 284.72, 285.98 and 288.38 eV has been presented in Fig. 2a. The major peak at 284.72 eV is exclusively assigned to carbon atoms (C–C bonding) in a pure carbon environment, i.e., amorphous carbons in our sample or adsorbed to the surface.[28] The peaks at 285.98 and 288.38 eV are ascribed to the existence of C–O/C–N and C=O/C=N bonds respectively.[29] N1s XPS spectra (Fig. 2b) indicate the co-existence of a number of distinguishable N environments fitting with three peaks in binding energies of 396.48, 398.52 and 399.95 eV. The two peaks at 398.86 and 399.95 eV can be assigned to N atoms in C=N–C microenvironment and tertiary nitrogen respectively.[30, 31] The peak at 396.48 eV may be attributed to Ti–N, implying that the conductivity could be improved in the hybrid. In Fig. 2c, the curve fitting of O1s spectra basically indicates three components centered at 529.94, 531.52 and 533.50 eV in the TNCH, which are attributed to Ti–O–Ti, Ti–O–C and C=O respectively.[29, 32] As indicated in Fig. 2d, the binding energies of Ti2p3/2 and 2p1/2 are centered at 458.36 and 464.00 eV, in agreement with those of Ti^{4+} in TiO_2.[33]

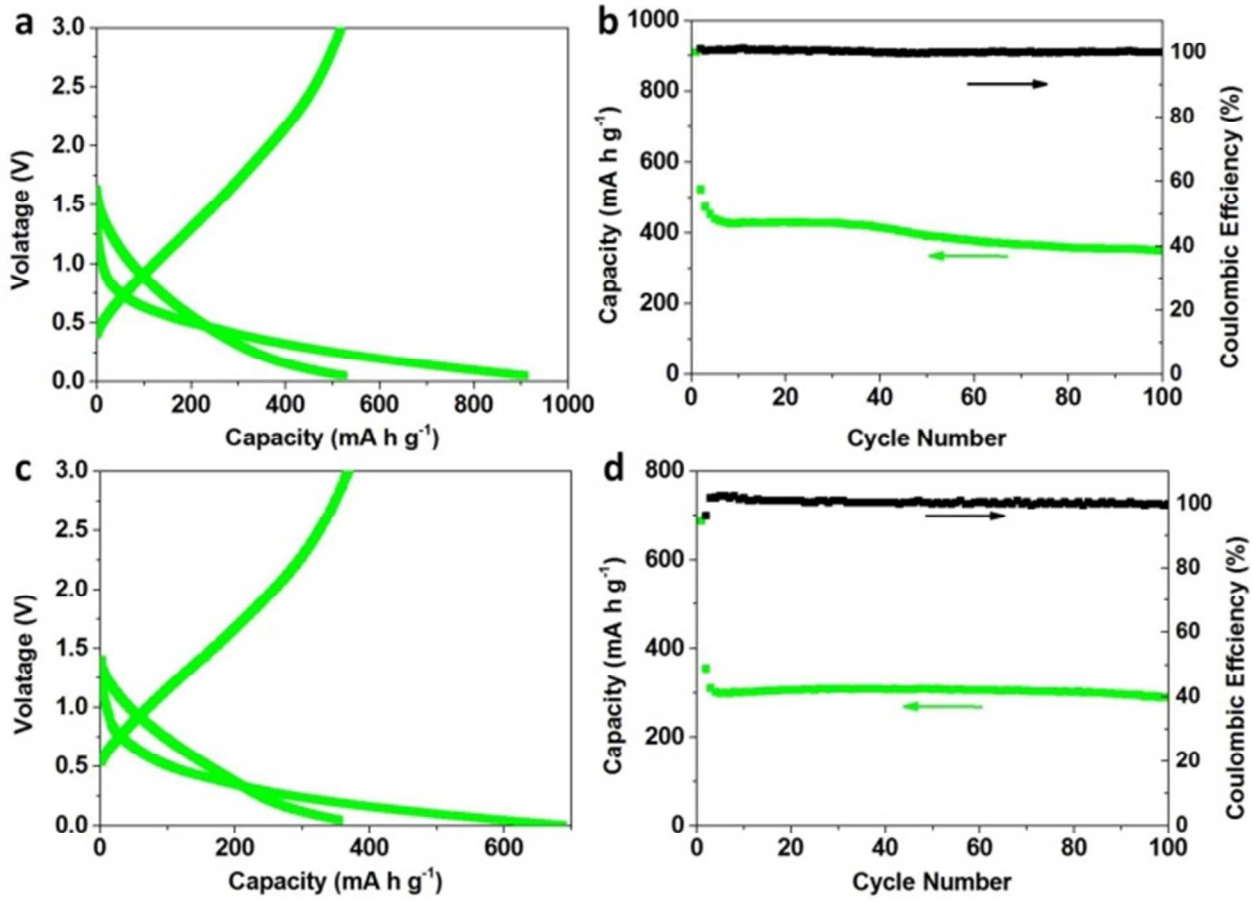

Fig. 3. Charge-discharge profiles, reversible capacities and Coulombic efficiency of TNCH at high rates of 2.0 A g^{-1} (a, b) and 5.0 A g^{-1} (c, d) respectively.

Journal Name

RSCPublishing

COMMUNICATION

The electrochemical studies of the TNCH using coin cells with Li metal slices serving as both the counter and reference electrodes at room temperature. More details are provided in the experimental section in Supporting Information. The cyclic voltammetric curve (Fig. S6) of electrode made of TNCH was determined at a scanning rate of 0.2 mV s^{-1}. The typical current curves are obvious with a voltage range of 0.01 V and 3 V, which show the insertion-deinsertion mechanism is very similar to graphene-based materials. The peak in 2nd cycle is lower than that in 1st cycle contributes the formation of solid electrolyte interface film.

Fig. 3a shows the first two charge–discharge voltage profiles for TNCH at a current density of 2.0 A g^{-1} between a voltage of 0.05 V and 3.00 V. These results demonstrate that TNCH has a typical discharge/charge characteristic of amorphous carbon. TNCH delivered a first-discharge capacity of 908.8 mA h g^{-1} and charge capacity of 518.3 mA h g^{-1}. The reversible capacity of TNCH anode at the second cycle is about 523.3 mA h g^{-1}, revealing a high Coulombic efficiency of 101%. Fig. 3b shows the Coulombic efficiency maintains nearly 100% at the second and the sequential cycles, which indicates that the formed interface is stable during cycling. After the 40th cycle, the discharge capacity of TNCH remains 414.4 mA h g^{-1}, which is higher than the theoretical capacity (372 mA h g^{-1}) of graphite. After the 100th cycle, the discharge capacity of TNCH still keeps 351.1 mA h g^{-1}.

A current density of 5.0 A g^{-1} is set to further investigate higher rate performance of TNCH. In Fig. 3c, the first-discharge capacity is 687.8 mA h g^{-1} with discharge cut-off voltages of 0.01 V in consideration of polarization potential at the high rate. The cut-off voltage range of 0.05−3 V is used in sequential cycles for comparing with the performance at 2 A g^{-1}. The discharge capacity of TNCH at the second cycle is 355 mA h g^{-1} with Coulombic efficiency of 96.2% because of higher discharge cut-off voltage of 0.05 V. Fig. 3d indicates the discharge capacity and Coulombic efficiency of TNCH also keep 288.4 mA h g^{-1} and ~ 100% respectively after the 100th cycle, much better than some reported amorphous carbon and graphite [34].

Comparative experiments were conducted to investigate the capacity of the material obtained in the absent of Ti^{4+} as crosslinking agent. The typical g-C_3N_4 sample obtained by annealing at 650 °C for 2 hour which has been confirmed by XRD analysis in Fig. S3. The g-C_3N_4 sample gives very lower capacities compared to the sample with Ti^{4+} shown in Fig. 4. The first discharge capacity is only 20.3 mA h g^{-1} and only less 4 mA h g^{-1} is retained after 5 cycles. Therefore, we conclude that Ti^{4+} not only plays an important role in the formation of stable TNCHs, but also catalyze g-C_3N_4 to form N-rich carbon hybrid with 3D channels.

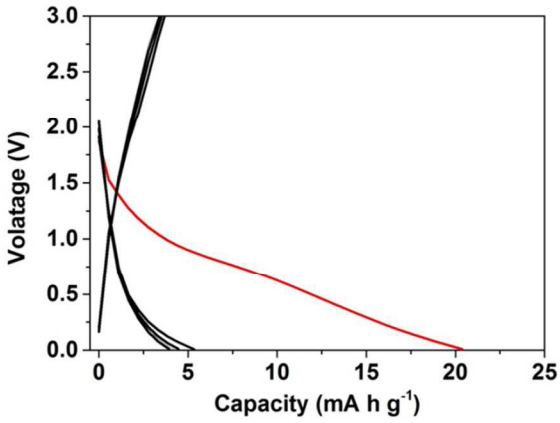

Fig. 4. Charge-discharge profiles of g-C_3N_4 obtained without titanate crosslinking agent at a rate of 0.1 A g^{-1}.

The excellent electrochemical performance of TNCH is probably rooted in its stable nano-architecture with the following features: 1) Titanate plays a propping role and improves the framework of TNCH which possesses 3D channels for lithium transport. 2) The existence of Ti–N bonding also enhances the conductivity of anode. 3) The usage of titanic acid can enhance the yield of g-C_3N_4 and TNCH to make their cost down. Therefore, the desired material could be applied into batteries or supercapacitors owing to superior performance for fast lithium storage.

Conclusions

In summary, we synthesized an amorphous N-rich titanate-carbon hybrid by one-pot solid state reaction with step-by-step heat treatments including polymerization and followed *in situ* carbonization at 500 and 650 °C respectively. The amorphous Ti-stable and N-rich framework provides stable 3D channels for lithium-ion transport. Therefore, electrochemical measurements demonstrate that this hybrid can deliver a reversible capacity of 523.3 mA h g^{-1} at high rate of 2.0 A g^{-1} much higher than theoretical value of graphite. Moreover, this hybrid anode also exhibits superior high-rate capability and cycling performance. The reported method provided new pathway to develop low cost and sustainable materials for fast lithium storage.

Acknowledgments

This research was supported by Natural Science Foundation of China (21303038), Heifei University of Technology start-up grant (407037069), and Hundred Talents Program of Anhui Province.

Notes and references

[a] Future Energy Laboratory, School of Materials Science and Engineering, Hefei University of Technology, Tunxi Road No.193 Hefei, Anhui, 230009, China. Email: liujh@hfut.edu.cn
[b] Department of Chemistry and Biochemistry, University of South Carolina, Columbia, SC 29208 United Statese.
[c] School of Chemical Engineering, Hefei University of Technology, Tunxi Road No.193 Hefei, Anhui, 230009, China

Electronic Supplementary Information (ESI) available: Experiment details, FTIR spectra, XRD curve, XPS spectrum and cyclic voltammetry curves. See DOI: 10.1039/c000000x/

1. C. N. R. Rao, K. Gopalakrishnan and A. Govindaraj, Nano Today, 2014, 9, 324-343.
2. I. V. Lightcap and P. V. Kamat, Acc. Chem. Res., 2013, 46, 2235-2243.
3. A. D. Roberts, X. Li and H. F. Zhang, Chem. Soc. Rev., 2014, 43, 4341-4356.
4. P. Barpanda, M. Ati, B. C. Melot, G. Rousse, J. N. Chotard, M. L. Doublet, M. T. Sougrati, S. A. Corr, J. C. Jumas and J. M. Tarascon, Nat. Mater., 2011, 10, 772-779.
5. H. G. Zhang, X. D. Yu and P. V. Braun, Nat. Nanotech., 2011, 6, 277-281.
6. H. Liu, F. C. Strobridge, O. J. Borkiewicz, K. M. Wiaderek, K. W. Chapman, P. J. Chupas and C. P. Grey, Science, 2014, 344.
7. Z. Y. Cao and B. Q. Wei, Energy Environ. Sci., 2013, 6, 3183-3201.
8. Q. Zhang, J. Q. Huang, W. Z. Qian, Y. Y. Zhang and F. Wei, Small, 2013, 9, 1237-1265.
9. H. Ota, Y. Sakata, A. Inoue and S. Yamaguchi, J. Electrochem. Soc., 2004, 151, A1659-A1669.
10. M. Lu, H. Cheng and Y. Yang, Electrochim. Acta, 2008, 53, 3539-3546.
11. L. G. Bulusheva, A. V. Okotrub, A. G. Kurenya, H. K. Zhang, H. J. Zhang, X. H. Chen and H. H. Song, Carbon, 2011, 49, 4013-4023.
12. K. N. Wood, R. O'Hayre and S. Pylypenko, Energy Environ. Sci., 2014, 7, 1212-1249.
13. J. H. Liu, J. S. Chen, X. F. Wei, X. W. Lou and X. W. Liu, Adv. Mater., 2011, 23, 998-1002.
14. J. H. Liu and X. W. Liu, Adv. Mater., 2012, 24, 4097-4111.
15. G. N. Zhu, Y. G. Wang and Y. Y. Xia, Energy Environ. Sci., 2012, 5, 6652-6667.
16. Y. Sun, L. Zhao, H. L. Pan, X. Lu, L. Gu, Y. S. Hu, H. Li, M. Armand, Y. Ikuhara, L. Q. Chen and X. J. Huang, Nat. Commun., 2013, 4, 1870.
17. Y. G. Guo, J. S. Hu and L. J. Wan, Adv. Mater., 2008, 20, 2878-2887.
18. D. H. Wang, D. W. Choi, J. Li, Z. G. Yang, Z. M. Nie, R. Kou, D. H. Hu, C. M. Wang, L. V. Saraf, J. G. Zhang, I. A. Aksay and J. Liu, ACS Nano, 2009, 3, 907-914.
19. J. Liang, Y. Zheng, J. Chen, J. Liu, D. Hulicova-Jurcakova, M. Jaroniec and S. Z. Qiao, Angew. Chem. Int. Ed., 2012, 51, 3892-3896.
20. G. Liu, P. Niu, C. H. Sun, S. C. Smith, Z. G. Chen, G. Q. Lu and H. M. Cheng, J. Am. Chem. Soc., 2010, 132, 11642-11648.
21. X. D. Zhang, X. Xie, H. Wang, J. J. Zhang, B. C. Pan and Y. Xie, J. Am. Chem. Soc., 2013, 135, 18-21.
22. P. Niu, L. C. Yin, Y. Q. Yang, G. Liu and H. M. Cheng, Adv. Mater., 2014, 26, 8046- 8052.
23. D. J. Martin, K. P. Qiu, S. A. Shevlin, A. D. Handoko, X. W. Chen, Z. X. Guo and J. W. Tang, Angew. Chem. Int. Ed., 2014, 53, 9240-9245.
24. G. H. Dong, Z. H. Ai and L. Z. Zhang, RSC Adv., 2014, 4, 5553-5560.
25. S. Kumar, T. Surendar, B. Kumar, A. Baruah and V. Shanker, RSC Adv., 2014, 4, 8132-8137.
26. F. He, G. Chen, Y. G. Yu, Y. S. Zhou, Y. Zheng and S. Hao, Chem. Commun., 2015, 51, 425-427.
27. J. H. Li, B. A. Shen, Z. H. Hong, B. Z. Lin, B. F. Gao and Y. L. Chen, Chem. Commun., 2012, 48, 12017-12019.
28. K. Dai, L. H. Lu, C. H. Liang, Q. Liu and G. P. Zhu, Appl. Catal. B-Environ., 2014, 156, 331-340.
29. J. Yu, G. Dai, Q. Xiang and M. Jaroniec, J. Mater. Chem., 2011, 21, 1049-1057.
30. S. W. Bian, Z. Ma and W. G. Song, J. Phys. Chem. C, 2009, 113, 8668-8672.
31. L. Ge and C. C. Han, Appl. Catal. B Environ., 2012, 117, 268-274.
32. J. G. Yu, H. G. Yu, B. Cheng, X. J. Zhao, J. C. Yu and W. K. Ho, J. Phys. Chem. B, 2003, 107, 13871-13879.
33. J. Wang, C. Fan, Z. Ren, X. Fu, G. Qian and Z. Wang, Dalton T., 2014, 43, 13783-13791.
34. Y. Fang, Y. Y. Lv, R. C. Che, H. Y. Wu, X. H. Zhang, D. Gu, G. F. Zheng and D. Y. Zhao, J. Am. Chem. Soc., 2013, 135, 1524-1530.

